

Errors in Predicting Muscle Fiber Lengths from Joint Kinematics Point to the Need to Include Tendon Tension in Computational Neuromuscular Models

Daniel A Hagen^a, Francisco J Valero-Cuevas^{a,b,*}

^a*Department of Biomedical Engineering, University of Southern California, Los Angeles, CA, USA*

^b*Division of Biokinesiology and Physical Therapy, University of Southern California, Los Angeles, CA, USA*

Keywords: kinematics, muscle fiber length, tendon dynamics, musculotendon, muscle mechanics, musculoskeletal modelling

University of Southern California

Department of Biomedical Engineering

Brain-Body Dynamics Lab

Ronald Tutor Hall, RTH-421

3710 S. McClintock Ave

Los Angeles, CA 90089-2905, USA

Phone: (213) 740-4219

Fax: (213) 821-5696

Website: ValeroLab.org

E-mail: valero@usc.edu

All authors were fully involved in the study and preparation of this preprint manuscript.

Accurate predictions of tendon forces must consider musculotendon mechanics; specifically muscle fiber lengths and velocities. These are either predicted explicitly by simulating musculoskeletal dynamics or approximated from measured limb kinematics. The latter is complicated by the fact that tendon lengths and pennation angles vary with both limb kinematics *and* tendon tension. We now derive the error in kinematically-approximated muscle fiber lengths as a general equation of muscle geometry and tendon tension. This enables researchers to objectively evaluate this error's significance—which can reach ~ 80% of the optimal muscle fiber length—with respect to the scientific or clinical question being asked. Although this equation provides a detailed functional relationship between muscle fiber lengths, joint kinematics and tendon tension, the parameters used to characterize musculotendon architecture are *subject-* and *muscle-*specific. This parametric uncertainty limits the accuracy of *any* generic musculoskeletal model that hopes to explain subject-specific phenomena. Nevertheless, the existence of such a functional relationship has profound implications to biological proprioception. These results strongly suggest that tendon tension information (from Golgi tendon organs) is likely integrated with muscle fiber length information (from muscle spindles) at the spinal cord to produce useful estimates of limb configuration to enable effective control of movement.

*Corresponding author

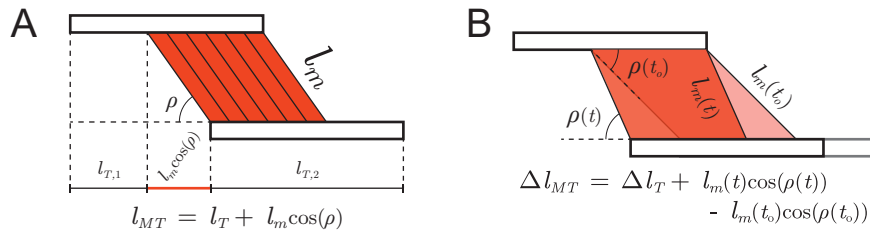


Figure 1: Approximation of musculotendon (MT) geometry as a flattened parallel bundle of pennated fibers in series with tendon (A) such that the change in length or *excursion* (Δl_{MT} , B) is defined as the sum of tendon length change (combining the tendons of origin and insertion, or $\Delta l_T = \Delta l_{T,1} + \Delta l_{T,2}$) and change in the portion of fiber length projected onto the line of action of the MT ($l_m(t) \cos(\rho(t)) - l_m(t_o) \cos(\rho(t_o))$) [1–3].

1. Introduction

Musculotendon (MT) complexes, as the name suggests, are composed of both muscle fibers *and* tendons [3]. These three-dimensional (often overlapping) bundles of fibers bulge, twist, and change lengths during contractions, but are conceptualized for simplicity as a flattened parallel bundle of fibers in series with an elastic element. This *parallelogram* simplification states that all fibers act in parallel *but* askew from the line of action by some pennation angle (ρ). This compartmentalizes the contributions of fiber length (l_m) and tendon length (l_T) to MT behavior (figure 1) [1–3]. Thus, MT length (l_{MT}) is defined as the sum of l_T (combining the tendons of origin and insertion; $l_T = l_{T,1} + l_{T,2}$) and the portion of l_m projected onto the line-of-action of the MT (figure 1A, equation (1)) [3].

$$l_{MT}(t) = l_T(t) + l_m(t) \cos(\rho(t)) \quad (1)$$

The excursion of the MT (Δl_{MT} , equation (2)) at time t is then defined as the difference between equation (1) evaluated at times t and t_o , such that l_m at time t is given by equation (3).

$$\Delta l_{MT}(t) = \Delta l_T(t) + l_m(t) \cos(\rho(t)) - l_m(t_o) \cos(\rho(t_o)) \quad (2)$$

$$l_m(t) = \frac{1}{\cos(\rho(t))} \left[\Delta l_{MT}(t) - \Delta l_T(t) \right] + \frac{\cos(\rho(t_o))}{\cos(\rho(t))} l_m(t_o) \quad (3)$$

In practice, MT excursion can be calculated from the measured kinematics of a movement¹. Even though l_m , l_T , and ρ are difficult to measure *in vivo* for a given subject, databases from imaging or cadaver studies can be used as approximations [4, 8–15]. This makes kinematics-based approximations for fiber lengths the most practical and most commonly used. These approximations further rely on the fundamental assumptions that tendons are inextensible (i.e., $\Delta l_T(t) \approx 0$) or that ρ is either constant ($\rho(t) \approx \rho_c$) or negligible ($\rho(t) \approx 0$).

¹I.e., by tracing the MT routing from its origin to insertion across postures (See [4]), or by calculating the integral of the moment arm functions for all joints crossed (See [5–7]). The latter approach does not consider how moment arms change with *respect to joint angles*. In *Appendix A.1*, we derive more accurate equations for MT length and velocity that account for this.

When *only* assuming inextensible tendons (*IT*), equation (3) simplifies to:

$$\tilde{l}_m^{IT}(t) \equiv \frac{\Delta l_{MT}(t)}{\cos(\rho(t))} + \frac{\cos(\rho(t_o))}{\cos(\rho(t))} l_m(t_o) \quad (4)$$

Alternatively, in the case where tendon stretch is included but ρ is assumed *constant* (*CP*), equation (3) simplifies to:

$$\tilde{l}_m^{CP}(t) \equiv \frac{1}{\cos(\rho_c)} [\Delta l_{MT}(t) - \Delta l_T(t)] + l_m(t_o) \quad (5)$$

More often, however, both assumptions are made and the kinematics-based approximation to fiber length simplifies equation (3) to:

$$\tilde{l}_m(t) \equiv \frac{\Delta l_{MT}(t)}{\cos(\rho_c)} + l_m(t_o) \quad (6)$$

which, in effect, has led the field to often equate fiber length changes to MT excursions for small pennation angles [16]².

Such approximations have greatly facilitated and enabled inferences regarding fiber lengths, velocities, or spindle (afferent) activity for multiple tasks [17–20]. Alternatively, the neuromechanical simulation software *OpenSim* offers a “stiff tendon” mode that makes similar assumptions [21]. In the aforementioned approaches, pennation angle is generally ignored or assumed constant. This practical approach to MT function has enabled computational studies to infer the neural control strategies of musculoskeletal systems [3, 16, 22–24], even though such models of muscle are known to be prone to parameter sensitivity [25, 26].

Here we explore how these approximations and sensitivities affect the conclusions that can be drawn from such muscle models—independently of the assumed contractile element. It is important to note that our analysis has implications to most lumped-parameter models (e.g., Hill-type models, [27]) and population-of-muscle-fibers models (e.g., the Fuglevand model, [28]) because such models tend to ignore tendon mechanics and consider pennation angles to be negligible. We first explicitly derive equations for the errors produced when making a variety of assumptions to enable the reader to make informed decisions about their impact on the particular scientific question or clinical condition studied. We then go on to explore the consequences to inter-muscle and inter-subject variability, and its impact on studies of neuromuscular control.

²While these two assumptions are typically made together, they have been separated here to demonstrate the relative error contribution for which each assumption accounts.

2. Methods

2.1. Derivation of Tendon Deformation as a Function of Tendon Forces

The elastic properties of collagen are such that tendon force (f_T) depends on tendon length (l_T), with a characteristic nonlinear “toe” region at low forces followed by a linear region at higher forces [3, 29–31]. To generalize this relationship across muscles, [31] modelled the *normalized* tendon force-length curve (equation (7a)) whereby f_T was normalized by the maximum isometric force of the muscle (i.e., $\hat{f}_T = f_T/F_{MAX}$) and l_T was normalized by the *optimal* tendon length (i.e., $\hat{l}_T = l_T/l_{T,o}$). Additionally, the parameters c^T , k^T , and L_r^T fit the asymptotic slope, curvature, and lateral-shift, respectively³. Note that [31] decided to normalize l_T by the *optimal* tendon length ($l_{T,o}$ — the tendon length when the muscle produces its maximal isometric force) instead of the slack length ($l_{T,s}$ — tendon length when tendon force is negligible) as it produced more “congruent curves.” However, the literature reports the ratio between tendon slack length and optimal muscle length [3, 32], so we preferred to normalize l_T by the slack length. The same relationship can be rewritten as equation (7b) for when l_T is normalized by $l_{T,s}$ instead (i.e., $\hat{l}_T' = (l_{T,s}/l_{T,o})\hat{l}_T$).

$$\hat{f}_T(t) = c^T k^T \ln \left\{ \exp \left[\frac{\hat{l}_T'(t) - L_r^T}{k^T} \right] + 1 \right\} \quad (7a)$$

$$= c^T k^T \ln \left\{ \exp \left[\frac{\left(\frac{l_{T,s}}{l_{T,o}}\right) \hat{l}_T(t) - L_r^T}{k^T} \right] + 1 \right\} \quad (7b)$$

This relationship, albeit *muscle*- and *subject*-specific, can be inverted to provide tendon length as a function of tendon force (equation (8))⁴.

$$\hat{l}_T(t) = \left(\frac{l_{T,o}}{l_{T,s}} \right) \left(k^T \ln \left\{ \exp \left[\frac{\hat{f}_T(t)}{c^T k^T} \right] - 1 \right\} + L_r^T \right) \quad (8)$$

Therefore, the normalized change in tendon length can be rewritten as a function of both the current and initial forces on the tendon (equation (9)).

$$\Delta \hat{l}_T(t) = k^T \left(\frac{l_{T,o}}{l_{T,s}} \right) \ln \left\{ \frac{\exp \left[\frac{\hat{f}_T(t)}{c^T k^T} \right] - 1}{\exp \left[\frac{\hat{f}_T(t_o)}{c^T k^T} \right] - 1} \right\} \quad (9)$$

2.2. Error in Fiber Length Approximations

To allow for better comparison across muscles, we define the relative errors in kinematically-approximated fiber lengths (denoted by η) as the differences between equation (3) and equations (4)–(6), normalized by optimal fiber

³See Appendix A.2 & A.3 for more in depth description of these parameters and their physiological ranges.

⁴Assuming that *rate*-specific phenomenon like *hysteresis*, *creep*, *force-relaxation* and *short-range stiffness* are negligible.

length ($l_{m,o}$). When assuming only IT , the error is defined by equation (10). Intuitively, this error will be equal to the tendon length change that was ignored (equation (9)), projected back onto the line of action of the fibers

$$\eta^{IT}(t) = (l_m(t) - \tilde{l}_m^{IT}(t)) / l_{m,o} \quad (10a)$$

$$= - \left(\frac{l_{T,s}}{l_{m,o}} \right) \frac{\Delta \hat{l}_T(t)}{\cos(\rho(t))} \quad (10b)$$

$$= - \left(\frac{l_{T,s}}{l_{m,o}} \right) \left(\frac{l_{T,o}}{l_{T,s}} \right) \frac{k^T}{\cos(\rho(t))} \ln \left\{ \frac{\exp \left[\frac{\hat{f}_T(t)}{c^T k^T} \right] - 1}{\exp \left[\frac{\hat{f}_T(t_o)}{c^T k^T} \right] - 1} \right\} \quad (10c)$$

Alternatively, when including tendon length changes but assuming CP the error is defined by equation (11).

$$\eta^{CP}(t) = (l_m(t) - \tilde{l}_m^{CP}(t)) / l_{m,o} \quad (11a)$$

$$= C_1(\rho(t), \rho_c) \left(\frac{\Delta l_{MT}(t) - \Delta l_T(t)}{l_{m,o}} \right) \quad (11b)$$

$$+ C_2(\rho(t), \rho(t_o)) \hat{l}_m(t_o)$$

Where C_1 reflects the proportion of $\Delta l_{MT} - \Delta l_T$ that was not projected back onto the line of action of the fibers but instead some other axis given by ρ_c (equation (12)) and C_2 represents the proportion of $l_m(t_o)$ incorrectly projected back onto the current line of action of the fibers (equation (13)).

$$C_1(\rho(t), \rho_c) = \frac{\cos(\rho_c) - \cos(\rho(t))}{\cos(\rho_c) \cos(\rho(t))} \quad (12)$$

$$C_2(\rho(t), \rho(t_o)) = \frac{\cos(\rho(t_o)) - \cos(\rho(t))}{\cos(\rho(t))} \quad (13)$$

These now allow the relative error in kinematically-approximated fiber lengths, $\eta(t)$, to be defined as equation (14).

Note that this error accounts for the proportions of Δl_{MT} and $l_m(t_o)$ that were not mapped onto the line of action of the

fibers (*CP* assumption) as well as the ignored tendon length change (*IT* assumption).

$$\eta(t) = (l_m(t) - \tilde{l}_m(t)) / l_{m,o} \quad (14a)$$

$$= C_1(\rho(t), \rho_c) \left(\frac{\Delta l_{MT}(t)}{l_{m,o}} \right) \left. \vphantom{C_1(\rho(t), \rho_c)} \right\} \begin{array}{l} \text{Error due to incorrectly projecting} \\ \text{MT excursion back onto the} \\ \text{line of action of the fibers} \end{array}$$

$$+ C_2(\rho(t), \rho(t_o)) \hat{l}_m(t_o) \left. \vphantom{C_2(\rho(t), \rho(t_o))} \right\} \begin{array}{l} \text{Error due to incorrectly projecting} \\ \text{initial fiber length back onto the} \\ \text{line of action of the fibers} \end{array} \quad (14b)$$

$$+ \eta^{IT}(t) \left. \vphantom{\eta^{IT}(t)} \right\} \begin{array}{l} \text{Error due to ignoring} \\ \text{tendon length change} \end{array}$$

Finally, correcting for this error provides a more accurate approximation of normalized fiber length that takes both limb kinematics and tendon tension in account (equation (15)).

$$\hat{l}_m(t) = \underbrace{\frac{1}{\cos(\rho(t))} \left(\frac{\Delta l_{MT}(t)}{l_{m,o}} \right)}_{\substack{\text{(Joint Kinematics)} \\ \text{Relative MT excursion projected back} \\ \text{onto the line of action of the fibers}}} + \underbrace{\frac{\cos(\rho(t_o))}{\cos(\rho(t))} \hat{l}_m(t_o)}_{\substack{\text{Initial fiber length} \\ \text{mapped onto the line} \\ \text{of action of the fibers}}} \quad (15)$$

$$- \underbrace{\left(\frac{l_{T,s}}{l_{m,o}} \right) \left(\frac{l_{T,o}}{l_{T,s}} \right) \frac{k^T}{\cos(\rho(t))} \ln \left\{ \frac{\exp \left[\frac{\hat{f}_T(t)}{c^T k^T} \right] - 1}{\exp \left[\frac{\hat{f}_T(t_o)}{c^T k^T} \right] - 1} \right\}}_{\substack{\text{(Tendon Tension)} \\ \text{Relative tendon length change projected back} \\ \text{onto the line of action of the fibers}}}$$

3. Results

3.1. Error from Ignoring Fiber Pennation

As the first two terms of (14b) illustrate, assuming that pennation angle is either constant or negligible will result in errors when approximating fiber lengths from limb kinematics [33]. The coefficient of the first term (C_1) reflects the percentage of Δl_{MT} that was not projected back onto the line of action of the fibers, but instead some other axis given by ρ_c (equation (12), figure 2). While this error will be negligible when $\rho(t) \approx \rho_c$, it is more sensitive to small changes in pennation as ρ_c increases (figure 3A)⁵. Therefore, when assuming CP for muscles with larger pennation

⁵ C_1 sensitivity can also be defined as the partial derivative of C_1 evaluated at ρ_c .

$$\left. \frac{\partial C_1}{\partial \rho} \right|_{\rho=\rho_c} = \tan(\rho_c) \sec(\rho_c) \quad (16)$$

Note that as ρ_c increases, so does the slope of C_1 evaluated at ρ_c , indicating that for the same small deviation from ρ_c , the proportion of Δl_{MT} that was incorrectly projected back onto the line of action of the fibers will increase as ρ_c increases.

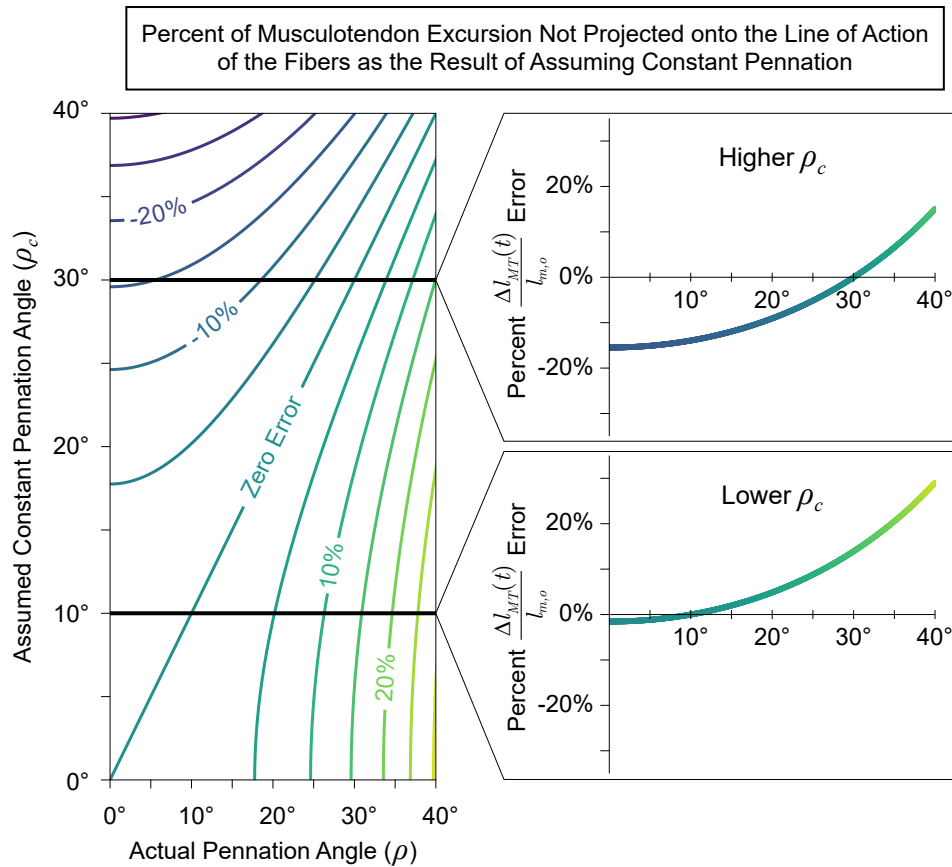


Figure 2: Contour map (*left*) for the percentage of musculotendon excursion that would be incorrectly mapped onto the line of action of the fibers (C_1) as the result of assuming some constant pennation angle as a function of the true pennation angle. For any assumed value of constant pennation (ρ_c), the resulting plot of C_1 is given by the corresponding horizontal cross-section of the contour plot. Examples of plots for lower and higher values of ρ_c are shown on the *right*. Note that the error is negligible when the true pennation angle is equal to the assumed value (diagonal line on the *left*, and zero-crossings on the *right*). Additionally, the error is less than $\pm 5\%$ when the assumed *and* actual pennation angles are less than $\sim 18^\circ$.

angles, the same deviation ($\rho = \rho_c \pm \delta\rho_1$) will result in a larger percentage of Δl_{MT} that was incorrectly projected back onto the line of action of the fibers.

The coefficient of the second term (C_2) reflects the percentage of $l_m(t_o)$ incorrectly projected back onto the line of action of the fibers as the result of assuming constant pennation (figure 4). Similar to C_1 , this error will be negligible when the pennation angle does not deviate from the initial value ($\rho(t) \approx \rho(t_o)$) and becomes more sensitive to changes in pennation as $\rho(t_o)$ increases (figure 3B)⁶. Therefore, when assuming CP for muscles with larger pennation angles that *also undergo larger pennation angle changes*, the same deviation ($\rho(t) = \rho(t_o) \pm \delta\rho_2$) will result in a larger percentage of $l_m(t_o)$ that was not projected back onto line of action of the fibers.

Reported average pennation angles vary across muscles in humans; from $\sim 1.3^\circ$ to $\sim 46.1^\circ$ in the lower limb [10, 34–36] and from $\sim 2.0^\circ$ to $\sim 33.0^\circ$ in the upper limb [14, 37–39] with large variability reported across subjects. Additionally, pennation angles have been reported to change by 120 to 175% from rest when the muscle is fully activated [38, 40–44]. Therefore, for some muscles and movements, the percentage of either Δl_{MT} or $l_m(t_o)$ that can be excluded or incorrectly mapped back onto the line of action of the fibers can be quite large ($\sim \pm 20\%$). As an example, [44] reported that the *medial gastrocnemius* experienced a $\Delta l_{MT} \approx -2$ cm during a maximum squat jump, where the pennation angle increased from 20° to 35° . If the pennation angle had been assumed to be constant and equal to the initial pennation angle (i.e., $\rho_c = \rho(t_o) = 20^\circ$), then 15.7% of Δl_{MT} and 14.7% of $l_m(t_o)$ would have been incorrectly mapped back onto the fiber, resulting in a normalized error of around -6.5% (-3.13mm) and 17.2% (8.24mm), respectively⁷.

3.2. Error from Assuming Inextensible Tendon

The third term of (14b) represents the error associated with assuming inextensible tendons [45]. Figure 5 shows equation (14b) evaluated at two initial tendon tensions. Note that when $\hat{f}_T = \hat{f}_T(t_o)$ (i.e., the normalized tendon force intercept), the tendon will have undergone a net zero length change and the error will be zero. However, notice that the slope at the intercept (red lines) demonstrates that starting at lower forces (i.e., an intercept towards the left) creates greater sensitivity to deviations from the initial tension, whereas at higher forces the sensitivity is lower and approaches the asymptotic slope (black arrows). Therefore, tasks that simulate non-isotonic tendon forces at low levels (like most activities of daily living) are at the greatest risk of errors of this type. However, the parameters used

⁶ C_2 sensitivity can also be defined as the partial derivative of C_2 evaluated at $\rho(t_o)$.

$$\left. \frac{\partial C_2}{\partial \rho} \right|_{\rho=\rho(t_o)} = \tan(\rho(t_o)) \quad (17)$$

Similar to C_1 , as $\rho(t_o)$ increases, so does the slope of C_2 evaluated at $\rho(t_o)$, indicating that for the same small deviation from $\rho(t_o)$, the proportion of $l_m(t_o)$ that was incorrectly projected back onto the muscle will increase as $\rho(t_o)$ increases.

⁷Given that $l_m(t_o) = 5.6$ cm and $l_{m,o} = 4.8$ cm [44]

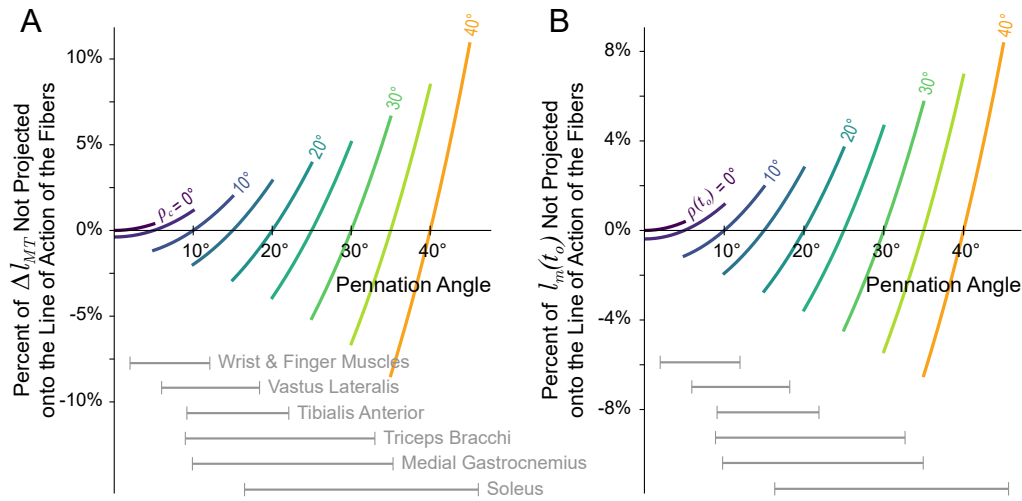


Figure 3: Sensitivity of the relative error coefficients C_1 (the proportion of MT excursion not projected back onto the line of action of the fibers, A) and C_2 (the proportion of the initial fiber length not projected back onto the line of action of the fibers, B) from equation (14). A small deviation ($\pm 5^\circ$) was applied to ρ_c or $\rho(t_o)$, respectively, and the resulting change in the coefficients were plotted. For (A), while the error is minimized when $\rho(t) = \rho_c$, as ρ_c increases the same deviation from the true pennation angle ($\rho(t) = \rho_c \pm 5^\circ$) will produce larger changes in C_1 and, therefore, a larger percentage of Δl_{MT} would be incorrectly projected back onto the line of action of the fibers. Similarly for (B), the error will be minimized when the pennation angle does not change from the initial value (i.e., $\rho(t) = \rho(t_o)$), but as $\rho(t_o)$ increases, the same deviation from the initial value ($\rho(t) = \rho(t_o) \pm 5^\circ$) will result in larger changes to C_2 and, therefore, a larger proportions of the initial fiber length would be incorrectly mapped back onto the fibers at time t . Ranges of pennation angles reported in the literature have been provide for a few muscle groups for reference [10, 14, 34–39].

to characterize the shape of the curves in figure 5 (i.e., c^T , k^T , $l_{T,o}/l_{T,s}$, and $l_{T,s}/l_{m,o}$) vary across muscles and subjects and can change with exercise, injury, or pathology [9, 46–52]. Additionally, ρ changes across muscles and subjects, as well as under different force levels for a given muscle (as previously stated) and will affect the error proportionally.

Therefore, we explored how changes in these parameters affect the magnitude of the error in fiber lengths by simulating isometric force tasks from rest. By doing so, MT excursion will be zero such that kinematically-approximated fiber lengths will be constant and the subsequent error will be identical to the normalized length change of the tendon, scaled by $l_{T,s}/l_{m,o}$ and divided by the cosine of the pennation angle. Figure figure 6A shows 10,000 random isometric force tasks (between 0-100% of maximum voluntary contraction, MVC) with the 5 parameters of interest uniformly sampled within their reported physiological ranges [53]⁸. Based on the reported range for $l_{T,o}/l_{T,s}$ (and the definitions of $l_{T,s}$ and $l_{T,o}$) the maximal normalized tendon deformation we can expect at MVC will be

$$\max_{MVC} \Delta \hat{l}_T = \frac{l_{T,o} - l_{T,s}}{l_{T,s}} = \frac{l_{T,o}}{l_{T,s}} - 1 \in [0.03, 0.07]$$

such that the maximal error in fiber length for this task will be the maximal tendon deformation scaled by the ratio $l_{T,s}/l_{m,o}$ and divided by the cosine of the pennation angle for a given muscle. For physiological ranges of these values,

⁸The range for ρ was chosen to be $< 40^\circ$ (See Section 3.1), the range for $l_{T,o}/l_{T,s}$ was chosen to be 1.03-1.07 [51, 52, 54], and the range for $l_{T,s}/l_{m,o}$ has been reported to be ≤ 11.25 [3, 55]. For an explanation of the physiological levels of c^T and k^T see Appendix A.3.

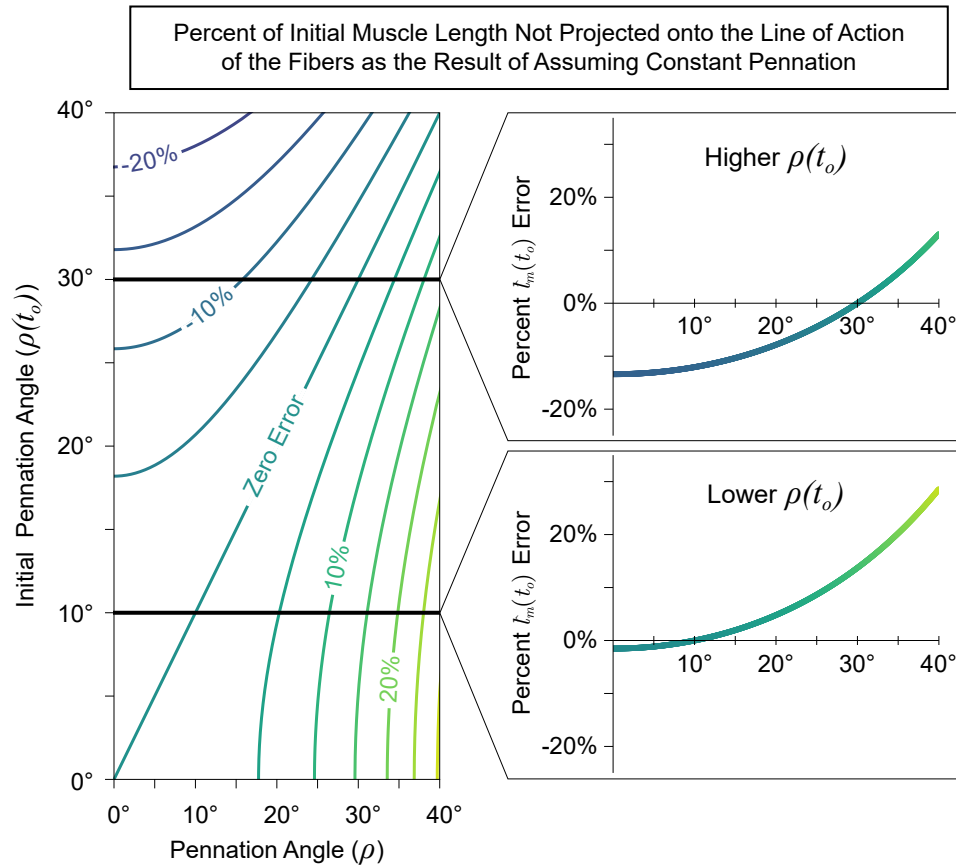


Figure 4: Contour map (*left*) for the percentage of initial fiber length that would be incorrectly mapped back onto the true line of action of the fibers (C_2) as the result of assuming some constant pennation angle as a function of the initial and current pennation angles. Regardless of the assumed constant pennation value, this error will depend on the amount by which the pennation angle changes from its initial value. Therefore, for some initial pennation angle, the resulting plot of the coefficient C_2 is given by the corresponding horizontal cross-section of the contour plot. Examples of plots for lower and higher values of $\rho(t_o)$ are shown on the *right*. Note that the error is negligible when the current pennation angle is equal to the initial pennation angle (diagonal line on the *left*, and zero-crossings on the *right*). Additionally, the error is less than $\pm 5\%$ when the initial *and* actual pennation angles are less than $\sim 18^\circ$. Therefore, for muscles with small pennation angles ($< 18^\circ$) that *do not drastically change* over the course of a movement, this error will be relatively small ($< \pm 5\%$).

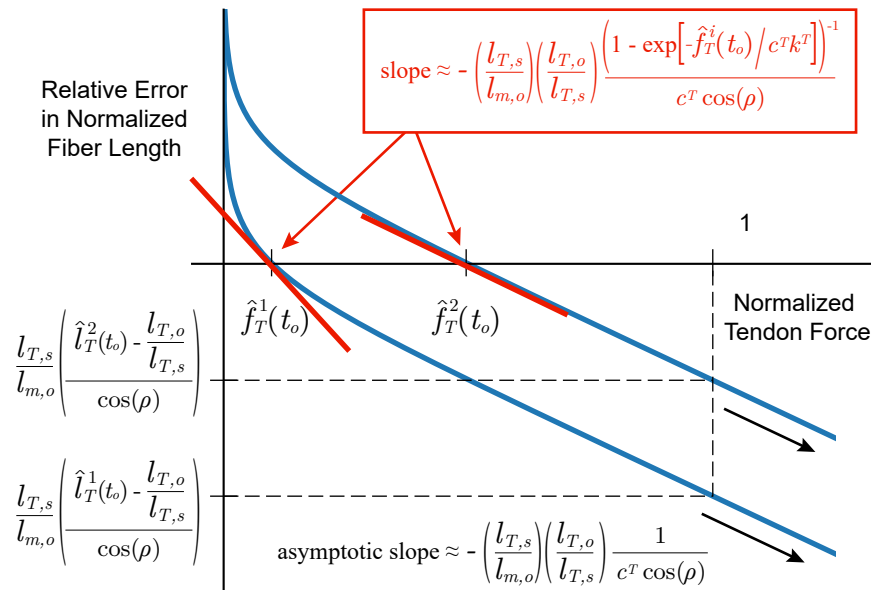


Figure 5: Relative error in fiber length as a result of assuming inextensible tendons (equation (10c)) that accounts for the previously ignored tendon length change, scaled by the tendon slack length to optimal fiber length ratio ($l_{T,s}/l_{m,o}$), and projected back onto the line of action of the fibers. Note that the error will be zero when the tension of the tendon is equal to the initial tension ($\hat{f}_T^i(t_o)$)—i.e., no net deformation of the tendon has occurred). Two different initial tension values have been chosen to demonstrate that starting at lower forces (i.e., an intercept towards the left) creates greater sensitivity to deviations from the initial tension, whereas at higher forces the sensitivity is lower and approaches the asymptotic slope (black arrows) where it will be proportional to $l_{T,s}/l_{m,o}$ and inversely proportional to $c^T = E \cdot CSA_T/F_{MAX}$ (i.e., the tendon’s normalized asymptotic stiffness).

the maximal error in fibers can reach magnitudes of $\sim 80\% l_{m,o}$. As expected, for higher tendon forces ($\geq 75\%$ of MVC) where \hat{l}_T converges to $l_{T,o}/l_{T,s}$, those trials with larger errors ($\geq 30\% l_{m,o}$) shows no clear dependence on c^T or k^T , but instead are determined by the product of $l_{T,o}/l_{T,s}$ and $l_{T,s}/l_{m,o}$ (figure 6B). Surprisingly, for lower tendon forces ($\leq 50\%$ of MVC), errors in fiber lengths $\geq 30\%$ (figure 6C) typically occur for musculotendons with *lower* normalized asymptotic tendon stiffness (*lower* c^T), *lower* “toe” region curvature in the tendon’s force-length curve (*higher* k^T), and higher ratios of tendon slack length to optimal muscle length ($l_{T,s}/l_{m,o} > 6$) and optimal tendon length to tendon slack length ($l_{T,o}/l_{T,s} > 1.04$). These parameters corresponds to a tendon that (i) is substantially longer than the muscle (i.e., larger $l_{T,s}/l_{m,o}$), (ii) can undergo relatively larger overall deformations (i.e., larger $l_{T,o}/l_{T,s}$), and (iii) has a *flatter* “toe” region in the tendon force-length curve. This “perfect storm” elicits disproportionately greater tendon deformations per unit force at lower forces. Conversely, if any of these conditions are not met, the errors in fiber lengths can be low ($\leq 5\% l_{m,o}$, figure 6A). Lastly, it is of course trivial to show from equations (2) & (3) that increasing the pennation angle will increase the proportion of Δl_T projected back onto the line of action of the fibers (i.e., a $1/\cos(\rho(t))$ function), and thus increase the magnitude of this error. However, we see that even muscles with low pennation angles are not immune to high errors (see second column from right in figure 6B,C). To further explore the consequences of varying these parameters during an isometric task, the reader is pointed to the online interactive

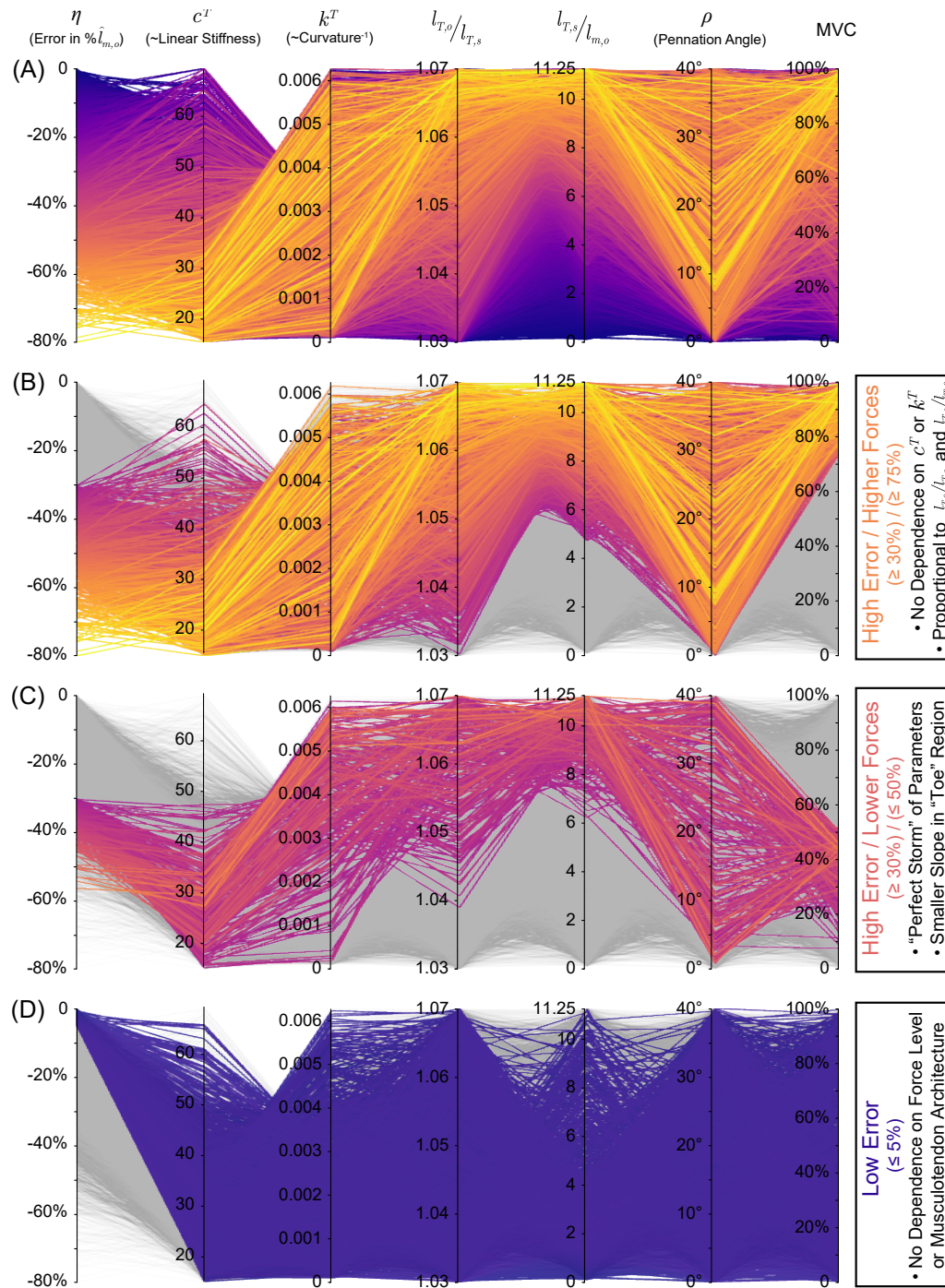


Figure 6: Parallel coordinates plot for the relative error in muscle fiber length (η) associated with assuming inextensible tendons for 10,000 random samples in the 5 parameters of interest (c^T , k^T , $l_{T,o}/l_{T,s}$, $l_{T,s}/l_{m,o}$, and ρ) within their reported physiological ranges during random isometric force tasks (top). As there is no MT excursion (Δl_{MT}) during an isometric contraction, assuming inextensible tendon is equivalent to assuming that muscle fiber length is constant at a given percentage of maximum voluntary contraction (MVC) and the error, therefore, will be identical to the normalized length change of the tendon, scaled by $l_{T,s}/l_{m,o}$ and $l_{T,o}/l_{T,s}$, and divided by the cosine of the pennation angle. For higher forces ($\geq 75\%$ MVC), we find that high errors ($\geq 30\%$ $l_{m,o}$) can occur for all values of c^T and k^T as, by definition, the tendon length converges to its optimal length (i.e., the error is only proportional to $l_{T,o}/l_{T,s}$ and $l_{T,s}/l_{m,o}$, second from top). Alternatively, we find that the error can be equally large for lower forces ($\leq 50\%$ MVC) when the tendon has low stiffness, low curvature (high radius of curvature), and larger ratios of $l_{T,s}$ to $l_{m,o}$ and $l_{T,o}/l_{T,s}$ (i.e., the “perfect storm”, second from bottom). Conversely, if any of these conditions are not met, the errors in muscle fascicle lengths can be low (bottom). Lastly, pennation angles do not appear to preclude any muscles from this sort of error, but it is trivial to show that increasing ρ will increase the proportion of Δl_T projected back onto the line of action of the muscle fascicles. Visit https://daniel8hagen.com/images/tendon_length_change_parallel_coords to access this interactive parallel coordinate plot online.

version of figure 6, available at https://daniel8hagen.com/images/tendon_length_change_parallel_coords.

4. Discussion

Biomechanics and neuromuscular control depend uniquely on the assumed properties of muscle. Chief among them is the dependence of muscle force for a given amount of neural drive on the lengths and velocities of its fibers. Our detailed analysis of how fiber lengths (and, by extension, velocities) are approximated from experimental data or simulations points to assumptions regarding musculotendon architecture (i.e., pennation angle and tendon elasticity) as the source of three dominant types of uncertainty and error (equation (14b)). More importantly, the magnitude of these errors is highly sensitive to the parameters characterizing musculotendon architecture. The significance of these potentially large errors is ultimately left to the modeller and their audience. To guide these decisions in practice, however, we provide a detailed presentation of the interactions between musculotendon architecture, musculotendon force magnitude, as well as its dependence on the ratios of tendon slack length to optimal fiber length and of optimal tendon length to tendon slack length. These high-dimensional interactions show that some combinations of parameters will produce (i) relatively low errors vs. (ii) a “perfect storm” where errors will be unacceptably large by any measure, even for relatively low force magnitudes. Our work highlights that extreme care must be taken when making such approximations in the context of the scientific question being asked, the muscles and tasks being studied, and the available experimental data.

We began by showing that, when approximating fiber lengths from the kinematics, separately assuming either constant pennation or inextensible tendons will incur distinct errors with respect to the ground truth. The magnitude of these errors are themselves highly sensitive to the parameters that characterize the musculotendon (i.e., fiber pennation angle and tendon elasticity).

It is intuitively obvious that assuming zero or constant pennation will incorrectly map the changes in musculotendon length and the initial fiber length onto the current line of action of the fibers. Our community has often assumed that this error is negligible for “small” pennation angles, which may be true (figure 3A). However, we show that starting at reasonably modest pennation angles of 20° , the sensitivity of the errors escalates exponentially to the point where a $\pm 5^\circ$ deviation from the assumed constant pennation angle can lead to $> 5\%$ of the musculotendon excursion to be unaccounted for in the fiber length approximation—with potentially important consequences to force-length and force-velocity calculations. Similarly, it is known that some muscles with modest pennation angles nevertheless undergo large changes in pennation during everyday movements [c. 120–175%, 38, 40–44]. In these cases, the amount of initial fiber length that is incorrectly mapped back onto the line of action of the fibers can be $\gg 4\%$ as calculated for a $\pm 5^\circ$ change in pennation (figure 3B) and can reach magnitudes on the order of $\sim 20\%$ (see [44] example in

Section 3.1). Both of these errors increase greatly for more pennate (and highly studied) muscles such as *tibialis anterior*, *triceps brachii*, *medial gastrocnemius*, or *soleus*. This highlights the need for perhaps unrealistically or impractically accurate measurements of muscle pennation angle (and their change during a task) to accurately simulate force production in these muscles when they are operating away from the plateau of the force-length curve, and most everywhere in the force-velocity curve.

Additionally, if one wanted to assume inextensible tendons, one must note that the errors in estimated fiber lengths are exacerbated at lower forces ($\leq 50\%$ of MVC) if the combination of parameters that characterize the tendon's normalized force-length relationship (i.e., its asymptotic stiffness, c^T , and its curvature constant, k^T) and the ratios of the tendon's slack length to the optimal fiber length ($l_{T,s}/l_{m,o}$) and optimal tendon length to tendon slack length ($l_{T,o}/l_{T,s}$) meet the “perfect storm” criteria (e.g., *soleus* muscle) [3, 51, 55]. That is, errors can be quite large for more compliant tendons (i.e., low values of c^T and high values of k^T) with moderately high values of $l_{T,s}/l_{m,o}$ and $l_{T,o}/l_{T,s}$ (figure 6C). Conversely, if *any* of these “perfect storm” conditions are not met, the error can potentially be small, as can be seen by the wide distribution of parameters that produce less than 5% error in fiber lengths in figure 6D. Therefore, it is important to understand how a *particular* choice of parameters can affect the robustness of a kinematics-based fiber length approximation by understanding how they will effect the shape of the tendon's force-length relationship and how deformations of tendon will subsequently produce scaled changes in fiber length.

The limitations of this study do not necessarily affect the validity of our results. For example, we did not consider more complex musculotendon architectures that do not reflect the simple parallelogram, and we ignored hysteresis, tendon creep, short-range stiffness, and force-relaxation. In fact, the added nonlinearities and state-dependence of these omissions suggest that we may, in fact, be underestimating these uncertainties and errors. By correcting for the errors explicitly derived here, we arrive at a more accurate approximation of fiber length that relies on both limb kinematics *and* tendon dynamics (equation (15)). This equation creates a functional relationship, through the limb kinematics, between fiber lengths and tendon tensions for concentric, eccentric and isometric contractions. However, in practice, its sensitivity to parameter values makes it all-but-impossible to use to recover specific musculotendon behavior without accurate *subject-* and *muscle-specific* parameters.

These results raise further important issues relevant to the role of muscle spindles to provide proprioception for neuromuscular control. In Nature, proprioception provides animals a robust awareness of the state of their body and of their relation to the environment. The muscle spindles embedded in the intrafusal fibers of muscle are known to provide information about the velocity and length of a muscle. Muscle spindles, by sensing along the line of action of the muscle fibers, are nevertheless subject to similar uncertainties and errors to those described above when estimating the length of the musculotendon. However, it stands to reason that the nervous system can learn to interpret

and integrate spindle signals to estimate the posture of the limb because their afferent signals are implicitly functions of the *subject-* and *muscle-specific* musculotendon parameters. Nevertheless, equation (15) points to the physical necessity of knowing tendon tension in addition to fiber length to accurately estimate length (and velocity) of the musculotendon—and therefore limb posture. We speculate that this obligatory functional relationship between fiber lengths and tendon tensions may point to an additional evolutionary pressure for Golgi tendon organs (mechanoreceptors for tendon tension) whose projection to the same spinal, sub-cortical and cortical areas would critically enable more accurate estimates of limb posture.

Data Accessibility. All data used in this paper were previously published.

Author Contributions. D.A.H and F.J.V.-C. designed the research; D.A.H. performed the research; D.A.H. and F.J.V.-C. analysed the data. All authors discussed the results and wrote the paper.

Competing Interests. We have no competing interests.

Funding. Research reported in this publication was supported by the National Institute of Arthritis and Musculoskeletal and Skin Diseases of the National Institutes of Health under award numbers R01 AR-050520 and R01 AR-052345 and by the National Institute of Neurological Disorders and Stroke of the National Institutes of Health under the award number R21-NS113613 to F.J.V.-C. This work was also supported by Department of Defense CDMRP Grant MR150091 and Award W911NF1820264 from the DARPA-L2M programme to F.J.V.-C.

Acknowledgements. We are grateful to Felix Zajac for inspiring this research and to Gerald Loeb for his seminal work on musculoskeletal systems and for his equation describing normalized tendon tension-deformation (derived in [31]) which allowed us to find an explicit form of this error. Additionally, we thank Akira Nagamori and Christopher Laine for their helpful feedback during early project development.

Disclaimer. The content of this endeavour is solely the responsibility of the authors and does not represent the official views of the National Institutes of Health or the Department of Defense.

A. Appendix

A.1. *New and Improved Equations for Musculotendon Length and Velocity*

When simulating muscle fiber and tendon behavior it is paramount to use accurate equations for musculotendon (MT) length (l_{MT}) and velocity (v_{MT}). Historically, l_{MT} has been calculated either by tracing the MT routing from origin to insertion across postures [4], or by approximating the MT excursion (s) induced by joint rotations at every

joint crossed [5–7]. The latter approach assumes constant moment arms such that the MT excursion produced by a joint’s rotation from neutral ($\theta - \theta_o$) would be equal to the arc length of a sector of a circle with radius equal to the moment arm (r , equation (18)). Therefore, l_{MT} is approximated as the sum of some neutral MT length ($l_{MT,o}$) and the MT excursions of all joints crossed (equation (19)). Note that the negative sign in the MT excursion equation ensures that for a positive joint rotation from neutral, a MT with a positive moment arm will shorten.

$$s \approx -r(\theta - \theta_o) \quad (18)$$

$$l_{MT} \approx l_{MT,o} - \sum_i r_i(\theta_i - \theta_{i,o}) \quad (19)$$

Musculotendon velocity (v_{MT}) is defined as the change in excursion due to joint rotation(s) over time (20a). For constant moment arms, this is approximated as the linear combination of joint velocities ($\dot{\theta}_i$) scaled by their moment arms (20b).

$$v_{MT} = \lim_{\Delta t \rightarrow 0} \sum_i \frac{\Delta s_i}{\Delta t} \quad (20a)$$

$$\approx - \sum_i \lim_{\Delta t \rightarrow 0} \frac{r_i \Delta \theta_i}{\Delta t} = - \sum_i r_i \dot{\theta}_i \quad (20b)$$

However, moment arms are not constant, and the equations for l_{MT} and v_{MT} must account for changes in moment arms with respect to joint angles. As a first approximation, previous work evaluated equation (20b) with posture dependent moment arms ($r_i(\theta_i)$, equation (21)) [18].

$$v_{MT} \approx - \sum_i r_i(\theta_i) \dot{\theta}_i \quad (21)$$

Integrating equation (21) with respect to time reveals that this approximation equates s_i to the integral of the moment arm function ($r_i(\theta_i)$) across some joint rotation from neutral ($\theta_i - \theta_{i,o}$, equation (22)).

$$l_{MT} \approx l_{MT,o} - \int_{t_o}^t \sum_i r_i(\theta_i) \dot{\theta}_i dt = l_{MT,o} - \sum_i \int_{\theta_{i,o}}^{\theta_i} r_i(\theta_i) d\theta_i \quad (22)$$

While equations (22 & (21) better approximate l_{MT} and v_{MT} , respectively, they fail to capture how moment arm values change *with respect to joint angles*. To capture this, we propose a new equation for l_{MT} that relies on the definition of *arc length in polar coordinates* (23).

$$l_{MT} = l_{MT,o} - \sum_i \int_{\theta_{i,o}}^{\theta_i} \text{sgn}(r_i(\theta_i)) \sqrt{(r_i(\theta_i))^2 + \left(\frac{\partial r_i}{\partial \theta_i}\right)^2} d\theta_i \quad (23)$$

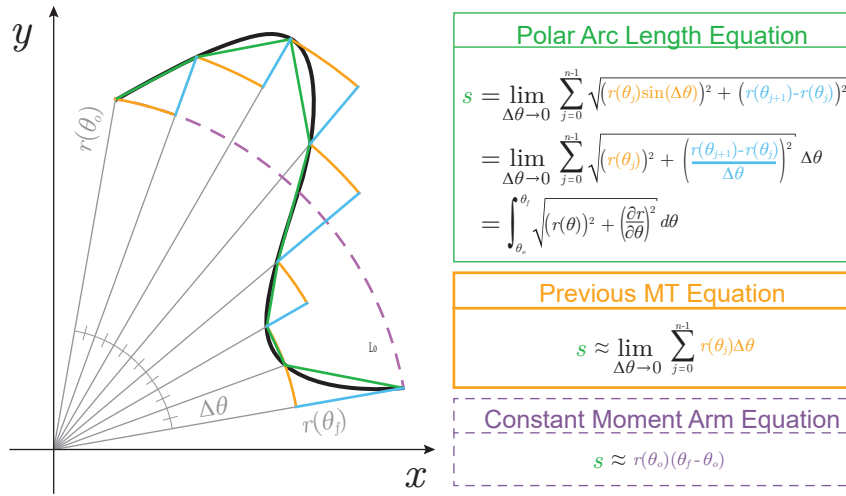


Figure 7: Evolution of MT excursion equations (s) and their differences. The constant moment arm equation [5–7] is the simplest approximation but clearly the arc length (*dashed purple*) does not accurately convey the true MT excursion (*black*). This was extended in [18] where the true arc length was approximated by integrating the posture-specific moment arm function (*orange*). Even for sufficiently small $\Delta\theta$, this approach does not completely capture the true MT excursion as it ignores the *change in moment arm with respect to the joint angle*. Correcting for this, we find the true MT excursion from the equation for arc length in polar coordinates (*green*). As the true MT excursion relies on the Euclidean of the moment arm and its partial derivative, the error between the approximation proposed in [18] and the true equation derived here can be bounded by the triangle inequality (see equation (25)).

Note that when moment arms are constant, equation (19) is recovered. The $\text{sgn}(r_{ij}(\theta_j))$ function returns +1 if $r_{ij}(\theta_j) > 0$ and -1 if $r_{ij}(\theta_j) < 0$ to recover the original relationship between joint rotations and excursion changes (i.e., positive joint rotation would shorten a MT with a positive moment arm). From equation (23) we derive the new equation for v_{MT} (24b).

$$v_{MT} = - \sum_i \frac{\partial}{\partial \theta_i} \left[\int_{\theta_{i,0}}^{\theta_i} \text{sgn}(r_i(\theta_i)) \sqrt{(r_i(\theta_i))^2 + \left(\frac{\partial r_i}{\partial \theta_i}\right)^2} d\theta_i \right] \frac{d\theta_i}{dt} \quad (24a)$$

$$= - \sum_i \text{sgn}(r_i(\theta_i)) \cdot \dot{\theta}_i \sqrt{(r_i(\theta_i))^2 + \left(\frac{\partial r_i}{\partial \theta_i}\right)^2} \quad (24b)$$

The relationship between excursions used in equations (19), (22), & (23) can be explained graphically in Figure 7 (*purple, orange, and green, respectively*).

By exploiting the limit definition of the integral terms for MT excursion, it is easy to show that the magnitude of

	$\Delta\theta_i > 0$	$\Delta\theta_i < 0$
$r_i(\theta_i) > 0$	$-\int_{\theta_{i,o}}^{\theta_i} \left \frac{\partial r_i}{\partial \theta_i} \right d\theta_i \leq \varepsilon_{MT,i} \leq 0$	$0 \leq \varepsilon_{MT,i} \leq -\int_{\theta_{i,o}}^{\theta_i} \left \frac{\partial r_i}{\partial \theta_i} \right d\theta_i$
$r_i(\theta_i) < 0$	$0 \leq \varepsilon_{MT,i} \leq \int_{\theta_{i,o}}^{\theta_i} \left \frac{\partial r_i}{\partial \theta_i} \right d\theta_i$	$\int_{\theta_{i,o}}^{\theta_i} \left \frac{\partial r_i}{\partial \theta_i} \right d\theta_i \leq \varepsilon_{MT,i} \leq 0$

Table 1: When calculating the MT excursion induced by the rotation of a joint, ignoring how much the moment arm (r_i) changes with respect to the joint angle (θ_i) will result in an *underestimate* of how much the MT has either *shortened* (red) or *lengthened* (blue). Whether or not a given joint rotation will caused shortening or lengthening depends on the sign of moment arm ($r_i(\theta_i)$) as well as the sign of the change in joint angle ($\Delta\theta_i$) [5]. Therefore, the associated error in the MT excursion ($\varepsilon_{MT,i}$) will have the same sign as the MT excursion and will be bounded by the intersection of this condition and equation (26) – which both change with the signs of $r_i(\theta_i)$ and $\Delta\theta_i$.

the error between equations (23) & (22), ε_{MT} , for each joint will be bounded by the triangle inequality (25).

$$\varepsilon_{MT} = - \sum_i \left(\int_{\theta_{i,o}}^{\theta_i} \text{sgn}(r_i(\theta_{i,j})) \sqrt{(r_i(\theta_i))^2 + \left(\frac{\partial r_i}{\partial \theta_i}\right)^2} d\theta_i - \int_{\theta_{i,o}}^{\theta_i} r_i(\theta_i) d\theta_i \right) \quad (25a)$$

$$= - \sum_i \text{sgn}(r_i) \int_{\theta_{i,o}}^{\theta_i} \left(\sqrt{(r_i(\theta_i))^2 + \left(\frac{\partial r_i}{\partial \theta_i}\right)^2} - |r_i(\theta_i)| \right) d\theta_i \quad (25b)$$

$$= \sum_i \varepsilon_{MT,i} \quad (25c)$$

$$\therefore |\varepsilon_{MT,i}| \leq \left| \int_{\theta_{i,o}}^{\theta_i} \left| \frac{\partial r_i}{\partial \theta_i} \right| d\theta_i \right| \quad (26)$$

$$\leq |r_i(\theta_i) - r_i(\theta_{i,o})| \quad (\text{when } r_i \text{ is monotonic on } [\theta_{i,o}, \theta_i]) \quad (27)$$

Note that the sign of the error will depend on the sign of the moment arm as well as the direction of the joint rotation such that sign of the error will be consistent with the sign of the MT behavior (i.e., *positive* for *lengthening* and *negative* for *shortening*). Therefore, errors of this type are always *underestimates* bounded between zero and equation (26) (the order of which depends on whether the joint rotation induced MT lengthening or shortening, table 1). Lastly, when r_i is either increasing or decreasing *only* during the joint rotation then this error is simply bounded between zero and the difference between the moment arm function evaluated at the initial and final posture (27).

A.2. Defining c^T and k^T

The tendon force-length relationship (given by [31], equation (7)) has fitting constants c^T , k^T , and L_r^T . As described in [31], these parameters affect the asymptotic slope of the linear region, the curvature of the plot, and the lateral-shift of the relationship, respectively. Additionally, by restricting c^T and k^T to $c^T k^T < 0.20$, L_r^T can be approximated as

$L_r^T \approx 1 - 1/c^T$ with $\approx 0.04\%$ error in L_r^T , allowing for the often-unknown fitting parameter space to be constrained to \mathbb{R}^2 . It can be shown from the limit of the slope of the *normalized* tendon force-length curve (equation (7)) as $\hat{l}_T \rightarrow \infty$ that c^T is proportional to the asymptotic slope (equation (28)).

$$\lim_{\hat{l}_T \rightarrow \infty} \frac{d\hat{f}_T}{d\hat{l}_T} = \lim_{\hat{l}_T \rightarrow \infty} c^T \left(\frac{l_{T,s}}{l_{T,o}} \right) \left[1 + \exp \left(\frac{L_r^T - \left(\frac{l_{T,s}}{l_{T,o}} \right) \hat{l}_T}{k^T} \right) \right]^{-1} = c^T \left(\frac{l_{T,s}}{l_{T,o}} \right) \quad (28)$$

Another generalization of the tendon force-length relationship is the *stress-strain curve* where stress is given by the force normalized by the tendon's physiological cross-sectional area ($\sigma = f_T/CSA_T$) and strain is given by the deformation of the tendon, normalized by the tendon's slack length ($\varepsilon = (l_T - l_{T,s})/l_{T,s}$) [3, 29, 51, 56]. This representation is useful for calculating the elastic modulus of tendon (E_T , Young's modulus for tendinous tissue) as the slope of the linear region.

$$E_T = \frac{\Delta\sigma}{\Delta\varepsilon} = \frac{\Delta f_T \cdot l_{T,s}}{CSA_T \cdot \Delta l_T} = \frac{f_{\max}}{CSA_T} \frac{\Delta \hat{f}_T}{\Delta \hat{l}_T} \quad (29)$$

As the slope of the linear region of (7) is given by $c^T(l_{T,s}/l_{T,o})$, we can rewrite c^T as (30). This equation expands upon the definition of c^T as the “linear stiffness” parameter and provides physical intuition about how changes in physiological parameters like tendon cross sectional area and muscle force producing capabilities will affect it.

$$c^T = \left(\frac{l_{T,o}}{l_{T,s}} \right) \frac{E_T \cdot CSA_T}{f_{\max}} \quad (30)$$

As the result of this relationship, tendon length changes at high forces can be approximated as

$$\Delta \hat{l}_T = \frac{1}{c^T} \left(\frac{l_{T,o}}{l_{T,s}} \right) \Delta \hat{f}_T \quad (31a)$$

$$= \frac{f_{\max}}{E \cdot CSA_T} \Delta \hat{f}_T \quad (31b)$$

How the fitting parameter k^T relates to the curvature of “toe” region of the normalized tendon force-length relationship is not explicitly clear. To explore the effect that changes in these parameters have on curvature, we define curvature as (32). This definition considers the amount of change that the tangent vector along a curve has in the direction of the normal vector. In the case where the curve is a circle, the curvature is defined as the inverse of the radius. Thus, as the radius *decreases*, the curvature *increases* and the “sharpness” of the curve increases. In the case where the radius becomes very large, the curvature goes to zero as the circle locally approaches a straight line. Therefore, large curvature values (κ) are associated with sharp changes along the curve. In mechanical systems, this

is often approximated as the second derivative of the curve.

$$\kappa = \frac{\partial^2 \hat{f}_T / \partial \hat{l}_T^2}{\left(1 + (\partial \hat{f}_T / \partial \hat{l}_T)^2\right)^{3/2}} \quad (32)$$

$$= \left(\frac{1}{c^T k^T}\right) \frac{(c^T (l_{T,s}/l_{T,o}))^2 \exp\left[\frac{L_r^T - (l_{T,s}/l_{T,o}) \hat{l}_T}{k^T}\right] \left(1 + \exp\left[\frac{L_r^T - (l_{T,s}/l_{T,o}) \hat{l}_T}{k^T}\right]\right)}{\left(\left(1 + \exp\left[\frac{L_r^T - (l_{T,s}/l_{T,o}) \hat{l}_T}{k^T}\right]\right)^2 + (c^T (l_{T,s}/l_{T,o}))^2\right)^{3/2}} \quad (33)$$

$$= \left(\frac{C_T}{c^T k^T}\right) \frac{z(1+z)}{\left((1+z)^2 + C_T\right)^{3/2}} \quad (34)$$

$$\left(\text{where, } z = \exp\left[\frac{L_r^T - (l_{T,s}/l_{T,o}) \hat{l}_T}{k^T}\right] \text{ and } C_T = (c^T (l_{T,s}/l_{T,o}))^2\right)$$

As k^T is defined as the variable that affects curvature (which varies along the continuous curve), we derive the maximum curvature of the tendon force-length curve in order to see the influence that k^T has on it. To do so, we take the derivative of (32) with respect to \hat{l}_T and find its zeros.

$$\frac{\partial \kappa}{\partial \hat{l}_T} = \frac{\partial \kappa}{\partial z} \frac{\partial z}{\partial \hat{l}_T} \quad (35a)$$

$$= -\left(\frac{C_T}{c^T k^T}\right) \left(\frac{l_{T,s}}{l_{T,o}}\right) z \cdot \left[\frac{(1+2z)((1+z)^2 + C_T)^{3/2} - 3z(1+z)^2((1+z)^2 + C_T)^{1/2}}{((1+z)^2 + C_T)^3}\right] \quad (35b)$$

$$= \frac{-\left(\frac{C_T}{c^T k^T}\right) \left(\frac{l_{T,s}}{l_{T,o}}\right) z}{\underbrace{\left((1+z)^2 + C_T\right)^{5/2}}_{\neq 0}} \cdot \underbrace{\left[(1-z)(1+z)^2 + C_T(1+2z)\right]}_{\text{max } \kappa \text{ when equal to zero.}} \quad (35c)$$

Therefore the curvature is at a maximum when

$$(1-z)(1+z)^2 + C_T(1+2z) = 0$$

which will occur when,

$$z^* = \frac{\sqrt[3]{2}(6C_T + 4)}{3\sqrt[3]{9C_T + 16 + j3\sqrt{3}\sqrt{32C_T^3 + 61C_T^2 + 32C_T}}} \quad (36)$$

$$+ \frac{\sqrt[3]{9C_T + 16 + j3\sqrt{3}\sqrt{32C_T^3 + 61C_T^2 + 32C_T}}}{3\sqrt[3]{2}} - \frac{1}{3}$$

Representing (36) in terms of magnitude and phase allows us to remove the imaginary component.

$$z^* = \frac{\sqrt[3]{2}(6C_T + 4)\sqrt[3]{9C_T + 16 - j3\sqrt{3}\sqrt{32C_T^3 + 61C_T^2 + 32C_T}}}{3\sqrt[3]{(9C_T + 16)^2 + 27(32C_T^3 + 61C_T^2 + 32C_T)}} \quad (37a)$$

$$+ \frac{1}{3\sqrt[3]{2}}\sqrt[3]{9C_T + 16 + j3\sqrt{3}\sqrt{32C_T^3 + 61C_T^2 + 32C_T}} - \frac{1}{3} \quad (37b)$$

$$= \frac{1}{3\sqrt[3]{2}}\left(\sqrt[3]{4(6C_T + 4)^3 e^{-j\phi}}\right)^{1/3} + \frac{1}{3\sqrt[3]{2}}\left(\sqrt[3]{4(6C_T + 4)^3 e^{j\phi}}\right)^{1/3} - \frac{1}{3} \quad (37c)$$

$$= \frac{2}{3}\sqrt[3]{6C_T + 4}\cos\left(\frac{\phi}{3}\right) - \frac{1}{3} \quad (37d)$$

$$\approx \sqrt{\frac{6C_T + 4}{3}} - \frac{1}{3} \approx \sqrt{2C_T} = c^T \left(\frac{l_{T,s}}{l_{T,o}}\right) \sqrt{2} \quad (37e)$$

$$\left(\text{where } \phi = \tan^{-1}\left(\sqrt{\frac{27(32C_T^3 + 61C_T^2 + 32C_T)}{(9C_T + 16)^2}}\right) \approx \pi/2\right)$$

Therefore the maximum curvature is given by plugging the (37c) into (34).

$$\max \kappa = \kappa \Big|_{z^*} \quad (38a)$$

$$= \left(\frac{C_T}{c^T k^T}\right) \frac{z^* (1 + z^*)}{((1 + z^*)^2 + C_T)^{3/2}} \quad (38b)$$

The approximate maximum curvature is found by instead evaluating the curvature at the approximate value for z^* (equation (37e)). If we make the reasonable assumption that $c^T \gg 10$ (see *Appendix A.3*), we can manipulate the

equation for maximal κ to find,

$$\max \kappa \approx \left(\frac{C_T}{c^T k^T} \right) \frac{\sqrt{2C_T} (1 + \sqrt{2C_T})}{\left((1 + \sqrt{2C_T})^2 + C_T \right)^{3/2}} \quad (39a)$$

$$= \left(\frac{C_T}{c^T k^T} \right) \frac{2C_T + \sqrt{2C_T}}{(3C_T + 2\sqrt{2C_T} + 1)^{3/2}} \quad (39b)$$

$$= \left(\frac{C_T}{c^T k^T} \right) \frac{2 \left(\sqrt{C_T} + \frac{\sqrt{2}}{4} \right)^2 - \frac{1}{4}}{3^{3/2} \left(\left(\sqrt{C_T} + \frac{\sqrt{2}}{3} \right)^2 + \frac{1}{9} \right)^{3/2}} \quad (39c)$$

$$\approx \left(\frac{C_T}{c^T k^T} \right) \left(\frac{2}{3\sqrt{3}} \right) \frac{1}{\sqrt{C_T} + \frac{\sqrt{2}}{3}} \quad (39d)$$

$$\approx \left(\frac{\sqrt{C_T}}{c^T k^T} \right) \left(\frac{2}{3\sqrt{3}} \right) \quad (39e)$$

$$\therefore \max \kappa \approx \left(\frac{2\sqrt{3}}{9} \right) \left(\frac{l_{T,s}}{l_{T,o}} \right) \frac{1}{k^T} \quad (39f)$$

$$(\max \kappa)^{-1} = \min R \approx \left(\frac{3\sqrt{3}}{2} \right) \left(\frac{l_{T,o}}{l_{T,s}} \right) k^T \quad (40)$$

Therefore, as equation (39f) suggests, the value of k^T is *inversely* proportional to the curvature and therefore proportional to the *radius* of curvature of the “toe” region (R), where small values of k^T correspond to high curvature or low radius of curvature (i.e., would exhibit *sharp transitions* from the “toe” region to the “linear” region). Additionally, equation (39f) and its reciprocal, equation (40), could be used to help find the hard-to-measure k^T constant from an experimental, normalized tendon force-length curve by either calculating the curvature and finding its maximum or by measuring the smallest radius of curvature, respectively.

A.3. Defining Physiological Ranges for c^T & k^T

The parameters that are used to characterize the *normalized* tendon force-length curve—asymptotic stiffness, the radius of curvature constant, and lateral shift (c^T , k^T , and L_r^T , respectively)—greatly influence the behavior of the tendon and vary across muscles, subjects, and sometimes tension rates [57, 58]. In order to determine the effects that changing these fitting parameters have on overall MT behavior, we define the physiological range for c^T and k^T from (i) the condition that $c^T k^T < 0.20$ [31], and (ii) the condition that, by definition, the tendon must be at its slack length ($\hat{l}_T = 1$) when normalized tendon force (\hat{f}_T) is near zero [3, 31, 32, 51]. The first constraint on c^T and k^T comes from [31], who stated that restricting values to $c^T k^T < 0.20$ allows L_r^T in equation (7) to be approximated as $L_r^T \approx 1 - 1/c^T$

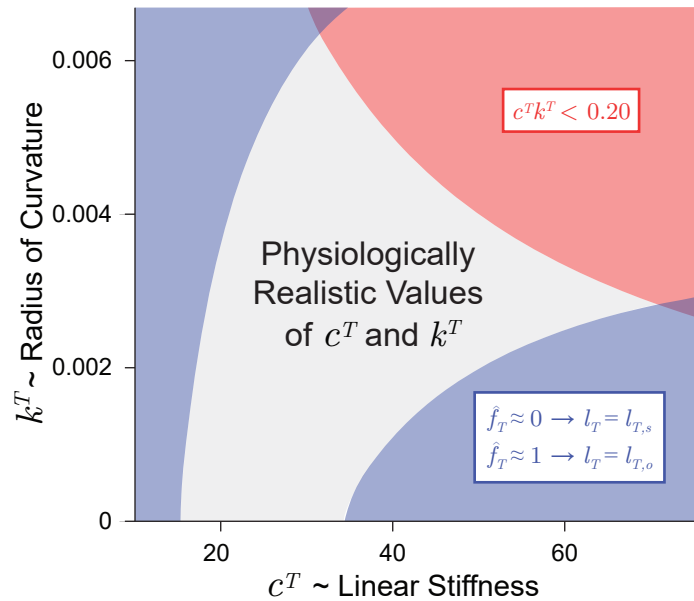


Figure 8: Physiologically realistic ranges for c^T and k^T under the assumptions that (i) $c^T k^T < 0.20$ (red) [31], and (ii), by definition, when force is negligible, tendon length equals its slack length (i.e., $\hat{f}_T \approx 0 \rightarrow \hat{l}_T \approx 1$, blue) [3, 31, 32, 51].

while incurring only a 0.04% error in L_r^T (red region excluded in figure 8). The second constraint produces a range of acceptable values of c^T and k^T when satisfying equation 8 for $\hat{f}_T \approx 0$ and $\hat{l}_T = 1$ and for $l_{T,s}/l_{T,o} \in [1.03, 1.07]$ (blue regions excluded in figure 8) [51, 52].

To validate the ranges produced by these constraints, we explore the reported ranges for c^T as (i) we can calculate c^T from Young's modulus (E), the tendon's physiological cross-sectional area (CSA_T), and the maximum isometric force of the muscle (f_{\max}) from equation 30 and (ii) the values of k^T are less often reported. Young's modulus has been reported to be conserved across muscles with the average E reported to be around 1.2 GPa and, therefore, changes to c^T can be attributed to changes in CSA_T and f_{\max} [3, 51, 59, 60]. These two parameters change across MTs as well as with training, injury, or pathology and help to explain the large variability in tendon stiffness seen across muscle and subjects [52, 61, 62]. As an example, Magnusson *et al.* calculated E , CSA_T , and f_{\max} for the *medial gastrocnemius* of 5 individuals during isometric contraction tasks [51] and the c^T values calculated from equation (30) ranged from 23.23 to 65.70 (37.47 ± 14.88). Therefore, the range of c^T values produced by the two constraints described above are consistent with values reported in the literature and are good first approximations of the range of physiological values when exploring the affect they have on tension-specific tendon deformation.

References

- [1] Carl Gans and Walter Bock. The functional significance of muscle architecture - a theoretical analysis. *Advances in Anatomy, Embryology and Cell Biology*, 38(April):115–142, 1965.

- [2] Carl Gans. Fiber architecture and muscle function, 1982. ISSN 0091-6331.
- [3] Felix E Zajac. Muscle and tendon: properties, models, scaling, and application to biomechanics and motor control. *Critical Reviews in Biomedical Engineering*, 17(4):359–410, 1989. URL <http://e.guigon.free.fr/rsc/article/Zajac89.pdf>.
- [4] DV Grieve. Prediction of gastrocnemius length from knee and ankle joint posture. *Biomechanics, A*, 2:405–412, 1978. URL <https://ci.nii.ac.jp/naid/10025974406/>.
- [5] Francisco J. Valero-Cuevas. *Fundamentals of Neuromechanics*, volume 8 of *Biosystems & Biorobotics*. Springer London, London, 2016. ISBN 978-1-4471-6746-4. doi: 10.1007/978-1-4471-6747-1. URL <http://link.springer.com/10.1007/978-1-4471-6747-1>.
- [6] Manish U. Kurse, Hod Lipson, and Francisco J. Valero-Cuevas. Extrapolatable analytical functions for tendon excursions and moment arms from sparse datasets. *IEEE Transactions on Biomedical Engineering*, 2012. ISSN 00189294. doi: 10.1109/TBME.2012.2189771.
- [7] K.N. An, Y. Ueba, E.Y. Chao, W.P. Cooney, and R.L. Linscheid. Tendon excursion and moment arm of index finger muscles. *Journal of Biomechanics*, 16(6):419–425, 1 1983. doi: 10.1016/0021-9290(83)90074-X. URL <http://linkinghub.elsevier.com/retrieve/pii/002192908390074X>.
- [8] Jeffery W Rankin and Richard R Neptune. Musculotendon lengths and moment arms for a three-dimensional upper-extremity model. *Journal of Biomechanics*, 45(9):1739–1744, 2012. doi: 10.1016/j.jbiomech.2012.03.010. URL http://ac.els-cdn.com/S0021929012001765/1-s2.0-S0021929012001765-main.pdf?_tid=68d430ec-785d-11e7-8e4b-00000aab0f6b&acdnat=1501773005_aef836f018a627424fd941cbc5f8b6e9.
- [9] Roland R. Roy and V. Reggie Edgerton. Skeletal Muscle architecture and performance. *Strength and Power in Sport*, pages 115–129, 1992.
- [10] Samuel R. Ward, Carolyn M. Eng, Laura H. Smallwood, and Richard L. Lieber. Are current measurements of lower extremity muscle architecture accurate? *Clinical Orthopaedics and Related Research*, 467(4):1074–1082, 2009. ISSN 15281132. doi: 10.1007/s11999-008-0594-8.
- [11] K N An, F. C. Hui, B F Morrey, R L Linscheid, and E Y Chao. Muscles across the elbow joint: A biomechanical analysis. *Journal of Biomechanics*, 14(10):659–669, 1981. ISSN 00219290. doi: 10.1016/0021-9290(81)90048-8. URL https://ac.els-cdn.com/0021929081900488/1-s2.0-0021929081900488-main.pdf?_tid=309fd37c-c8c9-11e7-a4e2-00000aacb35f&acdnat=1510615388_302f8cd8cbad026dcc3d5ecfe1271241.
- [12] V R Edgerton, P Apor, and R R Roy. Specific tension of human elbow flexor muscles. *Acta physiologica Hungarica*, 75(3):205–16, 1990. ISSN 0231-424X. URL <http://www.ncbi.nlm.nih.gov/pubmed/2392943>.
- [13] James A. Friederich and Richard A. Brand. Muscle fiber architecture in the human lower limb. *Journal of Biomechanics*, 23(1):91–95, 1990. ISSN 00219290. doi: 10.1016/0021-9290(90)90373-B.
- [14] Richard L. Lieber and Cynthia G. Brown. Quantitative method for comparison of skeletal muscle architectural properties. *Journal of Biomechanics*, 25(5):557–560, 1992. ISSN 00219290. doi: 10.1016/0021-9290(92)90096-J.
- [15] S H Scott, C M Engstrom, and G E Loeb. Morphometry of human thigh muscles. Determination of fascicle architecture by magnetic resonance imaging. *Journal of anatomy*, 182 (Pt 2:249–57, 1993. ISSN 0021-8782. URL <http://www.ncbi.nlm.nih.gov/pubmed/8376199%0Ahttp://www.pubmedcentral.nih.gov/articlerender.fcgi?artid=PMC1259835>.
- [16] Francisco J. Valero-Cuevas, Heiko Hoffmann, Manish U. Kurse, Jason J. Kutch, and Evangelos A. Theodorou. Computational Models for Neuromuscular Function. *IEEE Reviews in Biomedical Engineering*, 2009. ISSN 19411189. doi: 10.1109/RBME.2009.2034981.
- [17] Dimitar Stanev and Konstantinos Moustakas. Modeling musculoskeletal kinematic and dynamic redundancy using null space projection. *PLoS ONE*, 14(1):1–26, 2019. ISSN 19326203. doi: 10.1371/journal.pone.0209171.
- [18] Daniel A. Hagen and Francisco J. Valero-Cuevas. Similar movements are associated with drastically different muscle contraction velocities. *Journal of Biomechanics*, 59:90–100, 7 2017. ISSN 18732380. doi: 10.1016/j.jbiomech.2017.05.019. URL <http://linkinghub.elsevier.com/retrieve/pii/S0021929017302750>.

- [19] Jasmine A. Berry, Robert Ritter, Akira Nagamori, and Francisco J. Valero-Cuevas. The neural control of movement must contend with trajectory-specific and nonlinearly distorted manifolds of afferent muscle spindle activity. In *2017 International Joint Conference on Neural Networks (IJCNN)*, pages 1188–1194. IEEE, 5 2017. ISBN 978-1-5090-6182-2. doi: 10.1109/IJCNN.2017.7965987. URL <http://ieeexplore.ieee.org/document/7965987/>.
- [20] F J Valero-Cuevas, B A Cohn, H F Yngvason, and E L Lawrence. Exploring the high-dimensional structure of muscle redundancy via subject-specific and generic musculoskeletal models. *Journal of Biomechanics*, 48:2887–2896, 2015. doi: 10.1016/j.jbiomech.2015.04.026. URL http://ac.els-cdn.com/S0021929015002468/1-s2.0-S0021929015002468-main.pdf?_tid=10c0d784-785d-11e7-925f-00000aab0f27&acdnat=1501772857_f1b782a40301c37ac304ab7904aae70c.
- [21] Matthew Millard, Thomas Uchida, Ajay Seth, and Scott L Delp. Flexing Computational Muscle: Modeling and Simulation of Musculotendon Dynamics. *Journal of Biomedical Engineering*, 135(2):021005–021005, 2013. doi: 10.1115/1.4023390. URL <https://biomechanical.asmedigitalcollection.asme.org>.
- [22] Stephen H. Scott. Optimal feedback control and the neural basis of volitional motor control, 2004. ISSN 1471003X.
- [23] Michael I Jordan and Daniel M Wolpert. Computational motor control. *The Cognitive Neurosciences*, 1999.
- [24] Emanuel Todorov and Michael I. Jordan. Optimal feedback control as a theory of motor coordination. *Nature Neuroscience*, 2002. ISSN 10976256. doi: 10.1038/nm963.
- [25] Eric J. Perreault, Charles J. Heckman, and Thomas G. Sandercock. Hill muscle model errors during movement are greatest within the physiologically relevant range of motor unit firing rates. *Journal of Biomechanics*, 2003. ISSN 00219290. doi: 10.1016/S0021-9290(02)00332-9.
- [26] Carol Y. Scovill and Janet L. Ronsky. Sensitivity of a Hill-based muscle model to perturbations in model parameters. *Journal of Biomechanics*, 2006. ISSN 00219290. doi: 10.1016/j.jbiomech.2005.06.005.
- [27] A. V. Hill. The mechanics of active muscle. *Proceedings of the Royal Society of London. Series B, Containing papers of a Biological character. Royal Society (Great Britain)*, 141(902):104–117, 1953. ISSN 00804649. doi: 10.1098/rspb.1953.0027.
- [28] A. J. Fuglevand, D. A. Winter, and A. E. Patla. Models of recruitment and rate coding organization in motor-unit pools. *Journal of Neurophysiology*, 1993. ISSN 00223077. doi: 10.1152/jn.1993.70.6.2470.
- [29] Robert F Ker. Dynamic tensile properties of the plantaris tendon of sheep (*Ovis aries*). *The Journal of experimental biology*, 93:283–302, 1981. ISSN 0022-0949. URL <https://jeb-biologists-org.libproxy1.usc.edu/content/jexbio/93/1/283.full.pdfhttp://www.ncbi.nlm.nih.gov/pubmed/7288354>.
- [30] R. E. Shadwick. Elastic energy storage in tendons: Mechanical differences related to function and age. *Journal of Applied Physiology*, 1990. ISSN 01617567.
- [31] Ian E Brown, Stephen H Scott, and Gerald E Loeb. Mechanics of feline soleus: II Design and validation of a mathematical model. *Journal of Muscle Research and Cell Motility*, 17:221–233, 1996. URL <http://e.guigon.free.fr/rsc/article/BrownIEEtA196.pdf>.
- [32] U. Proske and D.L. Morgan. Tendon stiffness: Methods of measurement and significance for the control of movement. A review. *Journal of Biomechanics*, 20(1):75–82, 1 1987. ISSN 00219290. doi: 10.1016/0021-9290(87)90269-7. URL <https://linkinghub.elsevier.com/retrieve/pii/0021929087902697>.
- [33] Constantinos N. Maganaris, Vasilios Baltzopoulos, and Anthony J. Sargeant. In vivo measurements of the triceps surae complex architecture in man: Implications for muscle function. *Journal of Physiology*, 1998. ISSN 00223751. doi: 10.1111/j.1469-7793.1998.603be.x.
- [34] Tetsuo Fukunaga, Yoshiho Ichinose, Masamitsu Ito, Yasuo Kawakami, and Senshi Fukashiro. Determination of fascicle length and pennation in a contracting human muscle in vivo. *Journal of Applied Physiology*, 82(1):354–358, 1997. ISSN 8750-7587. doi: 10.1152/jappl.1997.82.1.354. URL <http://jap.physiology.org/cgi/content/full/82/1/354#BIBLhttp://jap.physiology.org/cgi/content/>

full/82/1/354.

- [35] GT Yamaguchi, AGU Sawa, D Moran, M Fessler, and JM Winters. A Survey of Human Musculotendon Actuator Parameters. *Multiple Muscle Systems: Biomechanics and Movement Organization*, pages 717–773, 1990.
- [36] D. C. Martin, M. K. Medri, R. S. Chow, V. Oxorn, R. N. Leekam, A. M. Agur, and N. H. McKee. Comparing human skeletal muscle architectural parameters of cadavers with in vivo ultrasonographic measurements. *Journal of Anatomy*, 199(4):429–434, 2001. ISSN 00218782. doi: 10.1046/j.1469-7580.2001.19940429.x.
- [37] Richard L. Lieber, Babak M. Fazeli, and Michael J. Botte. Architecture of selected wrist flexor and extensor muscles. *Journal of Hand Surgery*, 1990. ISSN 15316564. doi: 10.1016/0363-5023(90)90103-X.
- [38] R. D. Herbert and S. C. Gandevia. Changes in pennation with joint angle and muscle torque: in vivo measurements in human brachialis muscle. *The Journal of Physiology*, 484(2):523–532, 1995. ISSN 14697793. doi: 10.1113/jphysiol.1995.sp020683.
- [39] Li Khim Kwah, Rafael Z. Pinto, Joanna Diong, and Robert D. Herbert. Reliability and validity of ultrasound measurements of muscle fascicle length and pennation in humans: A systematic review, 2013. ISSN 87507587.
- [40] M. V. Narici, T. Binzoni, E. Hiltbrand, J. Fasel, F. Terrier, and P. Cerretelli. In vivo human gastrocnemius architecture with changing joint angle at rest and during graded isometric contraction. *Journal of Physiology*, 1996. ISSN 00223751. doi: 10.1113/jphysiol.1996.sp021685.
- [41] M V Narici, T Binzoni, E Hiltbrand, J Fasel, F Tettier, and P Cerretelli. Changes in human gastrocnemius architecture with joint angle at rest and with isometric contraction, evaluated in vivo. *Journal of Physiology (London)*, 496(1):287–297, 1996. URL <http://onlinelibrary.wiley.com/store/10.1113/jphysiol.1996.sp021685/asset/t.jp19964961287.pdf?v=1&t=jeq1eq63&s=892e4d35f1cd0696f53c4dd839bb36b7c253c0ea>.
- [42] Yasuo Kawakami, Yoshiho Ichinose, and Tetsuo Fukunaga. Architectural and functional features of human triceps surae muscles during contraction. *Journal of Applied Physiology*, 85:398–404, 1998. URL <http://jap.physiology.org/cgi/content/full/85/2/398>.
- [43] Constantinos N. Maganaris and Vasilios Baltzopoulos. Predictability of in vivo changes in pennation angle of human tibialis anterior muscle from rest to maximum isometric dorsiflexion. *European Journal of Applied Physiology and Occupational Physiology*, 79(3):294–297, 1999. ISSN 03015548. doi: 10.1007/s004210050510.
- [44] Sadao Kurokawa, Tetsuo Fukunaga, and Senshi Fukashiro. Behavior of fascicles and tendinous structures of human gastrocnemius during vertical jumping. *Journal of Applied Physiology*, 90(4):1349–1358, 2001. ISSN 8750-7587. doi: 10.1152/jappl.2001.90.4.1349. URL <http://www.jap.org>.
- [45] J. A. Hoffer, A. A. Caputi, I. E. Pose, and R. I. Griffiths. Roles of muscle activity and load on the relationship between muscle spindle length and whole muscle length in the freely walking cat. *Progress in Brain Research*, 1989. ISSN 18757855. doi: 10.1016/S0079-6123(08)62201-3.
- [46] G A Lichtwark and A M Wilson. Is Achilles tendon compliance optimised for maximum muscle efficiency during locomotion? *Journal of Biomechanics*, 40:1768–1775, 2007. doi: 10.1016/j.jbiomech.2006.07.025. URL www.elsevier.com/locate/jbiomech.
- [47] G A Lichtwark and A M Wilson. Optimal muscle fascicle length and tendon stiffness for maximising gastrocnemius efficiency during human walking and running. *Journal of Theoretical Biology*, 252(4):662–673, 2008. ISSN 1095-8541. doi: 10.1016/j.jtbi.2008.01.018.
- [48] Adamantios Arampatzis, Kiros Karamanidis, Gaspar Morey-Klapsing, Gianpiero De Monte, and Savvas Stafilidis. Mechanical properties of the triceps surae tendon and aponeurosis in relation to intensity of sport activity. *Journal of Biomechanics*, 40(9):1946–1952, 2006. URL <http://linkinghub.elsevier.com/retrieve/pii/S0021929006003320?showall=true>.
- [49] T Muraoka, T Muramatsu, T Fukunaga, and H Kanehisa. Elastic properties of human Achilles tendon are correlated to muscle strength. *Journal of Applied Physiology*, 99:665–669, 2005.
- [50] A. L. Hof, J. P. Van Zandwijk, and M. F. Bobbert. Mechanics of human triceps surae muscle in walking, running and jumping. *Acta Physiologica Scandinavica*, 174(1):17–30, 2002. ISSN 0001-6772. doi: 10.1046/j.1365-201x.2002.00917.x. URL <http://dare.ubvu>.

- vu.nl/bitstream/handle/1871/40141/HofZanBob2002.pdf?sequence=1.
- [51] S. Peter Magnusson, Per Aagaard, Sofie Rosager, Poul Dyhre-Poulsen, and Michael Kjaer. Load-displacement properties of the human triceps surae aponeurosis *in vivo*. *The Journal of Physiology*, 531(1):277–288, 2001. ISSN 00223751. doi: 10.1111/j.1469-7793.2001.0277j.x. URL <http://doi.wiley.com/10.1111/j.1469-7793.2001.0277j.x>.
- [52] Constantinos N. Maganaris and John P. Paul. Tensile properties of the *in vivo* human gastrocnemius tendon. *Journal of Biomechanics*, 35(12):1639–1646, 2002. ISSN 00219290. doi: 10.1016/S0021-9290(02)00240-3.
- [53] Veronica J. Santos, Carlos D. Bustamante, and Francisco J. Valero-Cuevas. Improving the fitness of high-dimensional biomechanical models via data-driven stochastic exploration. *IEEE Transactions on Biomedical Engineering*, 2009. ISSN 00189294. doi: 10.1109/TBME.2008.2006033.
- [54] Ernest J Cheng, Ian E Brown, and Gerald E Loeb. Virtual muscle: a computational approach to understanding the effects of muscle properties on motor control. *Journal of Neuroscience Methods*, 101:117–130, 2000. URL <http://ami.usc.edu/mddf/virtualmuscle>.
- [55] Melissa G Hoy, Felix E Zajac, and Michael E Gordon. A Musculoskeletal Model of the Human Lower Extremity: The Effect of Muscle, Tendon, and Moment Arm on the Moment-Angle Relationship of Musculotendon Actuators at the Hip, Knee, and Ankle. *Journal of Biomechanics*, 23(2):157–169, 1990.
- [56] W C Herrick, H B Kingsbury, and D. Y.S. Lou. A study of the normal range of strain, strain rate, and stiffness of tendon. *Journal of Biomedical Materials Research*, 12(6):877–894, 1978. ISSN 10974636. doi: 10.1002/jbm.820120610.
- [57] Constantinos N Maganaris and John P Paul. Hysteresis measurements in intact human tendon. *Journal of Biomechanics*, 33(12):1723–1727, 2000. ISSN 00219290. doi: 10.1016/S0021-9290(00)00130-5.
- [58] Taija Finni, Jussi Peltonen, Lauri Stenroth, and Neil J. Cronin. Viewpoint: On the hysteresis in the human Achilles tendon. *Journal of Applied Physiology*, 114(4):515–517, 2013. ISSN 8750-7587. doi: 10.1152/jappphysiol.01005.2012. URL <http://www.jappphysiol.org>.
- [59] M. B. Bennett, R. F. Ker, Nicola J. Imery, and R. Mc N. Alexander. Mechanical properties of various mammalian tendons. *Journal of Zoology*, 209(4):537–548, 1986. ISSN 14697998. doi: 10.1111/j.1469-7998.1986.tb03609.x.
- [60] C. M. Pollock and R. E. Shadwick. Relationship between body mass and biomechanical properties of limb tendons in adult mammals. *American Journal of Physiology-Regulatory, Integrative and Comparative Physiology*, 2017. ISSN 0363-6119. doi: 10.1152/ajpregu.1994.266.3.r1016.
- [61] A L Hof. *In vivo* measurement of the series elasticity release curve of human triceps surae muscle. *Journal of Biomechanics*, 31(9):793–800, 1998. ISSN 00219290. doi: 10.1016/S0021-9290(98)00062-1. URL <http://e.guigon.free.fr/rsc/article/Hof98.pdf>.
- [62] G. A. Lichtwark and A.M. Wilson. *In vivo* mechanical properties of the human Achilles tendon during one-legged hopping. *Journal of Experimental Biology*, 208(24):4715–4725, 2005. ISSN 0022-0949. doi: 10.1242/jeb.01950.